

Article

Effect of Thermal Radiation and Double-Diffusion Convective Peristaltic Flow of a Magneto-Jeffrey Nanofluid through a Flexible Channel

Asha S. Kotnurkar ^{1,*}, Joonabi Beleri ¹, Irfan Anjum Badruddin ^{2,*}, Khaleed H.M.T. ³, Sarfaraz Kamangar ² and Nandalur Ameer Ahammad ⁴

¹ Department of Studies and Research in Mathematics, Karnatak University, Dharwad 580003, India; joonabibeleri@kud.ac.in

² Mechanical Engineering Department, College of Engineering, King Khalid University, Abha 61411, Saudi Arabia; sarfaraz.kamangar@gmail.com

³ Department of Mechanical Engineering, Faculty of Engineering, Islamic University of Madinah, Madinah Munawara 42351, Saudi Arabia; khalid_tan@iu.edu.sa

⁴ Department of Mathematics, Faculty of Science, University of Tabuk, Tabuk 71491, Saudi Arabia; anaudalur@ut.edu.sa

* Correspondence: ashask@kud.ac.in (A.S.K.); magami.irfan@gmail.com (I.A.B.)

Abstract: The noteworthiness of double-diffusive convection with magneto-Jeffrey nanofluid on a peristaltic motion under the effect of MHD and porous medium through a flexible channel with the permeable wall has been theoretically examined. A non-linearized Rosseland approximation is utilized to show the thermal radiation effect. The governing equations are converted to standard non-linear partial differential equations by using suitable non-dimensional parameters. Solutions of emerging equations are obtained by using the multi-step differential transformation method (MS-DTM). The differential transformation method (DTM) can be applied directly to nonlinear differential equations without requiring linearization and discretization; therefore, it is not affected by errors associated with discretization. The role of influential factors on concentration, temperature, volume fraction, and velocity are determined using graphs. A significant outcome of the present article is that the presence of double-diffusive convection can change the nature of convection in the system. The present results have a wide biological applicability, including for biomicrofluidic devices that regulate the fluid flow through a flexible endoscope and other medical pumping systems.

Keywords: peristaltic flow; double diffusion; Jeffrey nanofluid; magnetic field; thermal radiation; porous media; flexible channel; permeable walls; MS-DTM

MSC: 76XX; 76DXX; 76RXX; 76SXX; 76VXX; 76WXX



Citation: Kotnurkar, A.S.; Beleri, J.; Badruddin, I.A.; H.M.T., K.; Kamangar, S.; Ahammad, N.A. Effect of Thermal Radiation and Double-Diffusion Convective Peristaltic Flow of a Magneto-Jeffrey Nanofluid through a Flexible Channel. *Mathematics* **2022**, *10*, 1701. <https://doi.org/10.3390/math10101701>

Academic Editor: Carlos Llopis-Albert

Received: 6 March 2022

Accepted: 19 April 2022

Published: 16 May 2022

Publisher's Note: MDPI stays neutral with regard to jurisdictional claims in published maps and institutional affiliations.



Copyright: © 2022 by the authors. Licensee MDPI, Basel, Switzerland. This article is an open access article distributed under the terms and conditions of the Creative Commons Attribution (CC BY) license (<https://creativecommons.org/licenses/by/4.0/>).

1. Introduction

Peristaltic transport is currently one of the most important pumping mechanisms due to its many applications in engineering, medical sciences, and biomechanics. The mechanism of peristalsis is due to a wave transmission along a tube wall or channel. The word “peristalsis” is derived from the Greek word “peristaltikos”, meaning clasp and compression. In 1966, Latham [1] introduced peristalsis, and the motion is the principle behind many devices, including heart–lung machines and finger and roller pumps. The processes of oxygenation and haemodialysis are biologically significant. Further, Shapiro et al. [2] analysed peristaltic pumping with long wavelengths at a low Reynolds number. Jaffrin et al. [3] demonstrated the mechanism of peristaltic flow in Newtonian and non-Newtonian fluids. The study of Non-Newtonian fluid transport phenomena has increased considerably due to their importance in biological and industrial applications. The relationship between shear stress and shear rate is not linear in a non-Newtonian fluid.

Examples of non-Newtonian liquids are polymer solutions, starch suspensions, molten polymers, shampoo, and blood. An important class of these non-Newtonian fluids constitutes the linear viscoelastic model. Jeffrey fluid is a viscoelastic fluid model in which viscosity remains constant and shear rate is time dependent. Among several non-Newtonian liquid models, Jeffrey fluid model has gained attention from many investigators. Further, Khan et al. [4] studied Unsteady flows of a Jeffrey fluid between two side walls over a plane wall. Baranovskii [5] analysed the stationary motion equations of Jeffrey's viscoelastic medium in an inhomogeneous boundary value problem. Baranovskii [6] analysed the optimal control for steady flows of the Jeffrey's fluids with slip boundary condition. Baranovskii [7] also studied the Global solutions for a model of polymeric flows with wall slip. Hayat et al. [8] Effect of magnetic field on the peristalsis involving Jeffrey fluid.

Researchers have discovered a number of methods to improve the thermophysical characteristics of fluids in recent years. Adding tiny solid particles with enhanced heat conductivity to fluid is one such method [9]. A fluid suspension containing microparticles or larger particles is unstable and has flow resistance. Surface roughness and clotting can occur when such fluids are introduced in human body. However, a suspension with nanosized particles, from 1 to 100 nm, cover a greater surface area and enhance conduction and convection coefficients. Nanoparticles have significant applications in industries such as engineering. In biomedical fields, cancer therapy using targeted drug delivery involves a nanofluid. The current state of nanofluids research has been made possible by extensive research. Akbar et al. [10] analysed the slip effects on the peristaltic movement of nanofluid. Recently, Ayub et al. [11] showed the impact of thermal radiation in mixed convection peristaltic movement of a third-grade nanoliquid. Further, Asha et al. [12] analysed the peristaltic propulsion of a Carreau nanoliquid under the presence of Joule heating in an inclined asymmetric channel.

The double-diffusion concept is found when fluid movement occurs through with thermal and concentration gradient. In 1976, Aifantis [13] was the first to propose the concept of the double-diffusive model. If a constant temperature difference is maintained, this thermal diffusion in a mixture will produce a concentration gradient in a fluid. Double-diffusive convection is an important concept for understanding industrial, engineering, and biomedical problems. Because of the application of double diffusion in biomedicine, researchers have taken a keen interest in understanding double diffusion at low Reynolds numbers. Peristaltic flow with diffusion convection has found applications in the biomedical domain. Ganesan et al. [14] analysed the impact of thermal radiation and double diffusion in non-Newtonian fluids. Further, Raju et al. [15] combined impact of induced Brownian motion, thermophoresis, and magnetic fields on double stratified nonlinear thermal radiation. The analytical results of double-diffusive convective flow by considering non-Newtonian fluid are given in references [16–19].

Darcy's law applies to a porous medium. A flexible channel is a geometry with porous walls that expand and contract. Over the last few decades, there have been many investigations into porous media because of its importance in industrial and biological processes. These include the study of Hussain et al. [20], who investigated the impact of nonlinear radiation of peristaltic pumping by considering hydromagnetic fluids in a porous medium. They found that pressure gradient rises due to the Darcy parameter. The peristaltic movement of the non-Newtonian model liquid along with a porous medium in a channel was investigated by Ramesh et al. [21]. Some recent research on porous medium in peristaltic flow, considering Newtonian and non-Newtonian fluids, was studied by Vajravelu et al. [22], Maiti et al. [23], and Nooren et al. [24]. Thermal convection in electrically conducting liquid in a porous media under the impact of the external magnetic field has attracted many researchers in the past few decades due to the importance of new porous materials. Recently, Hasona et al. [25] examined the impact of MHD on peristaltic movement. Under multiple conditions, other studies based on numerical methods and experiments have also been described.

In the view of the above literature, the current study shows the application of double-diffusive convective flow and thermal radiation effects in peristaltic nanofluid movement through flexible channels from a mathematical perspective. The present results have broad applications in biological functions, such as biomicrofluidic devices that regulate the fluid flow through a flexible endoscope and another medical pumping systems. In recent years, there has been a lack of focus on developing and applying analytical and numerical approaches. Such strategies can help to overcome the complexity and non-linearity seen in non-Newtonian liquids. Peristaltic mechanisms with non-Newtonian liquids necessitate substantially non-linear partial differential equations. It is hard to find precise answers to such challenges. We employed a semi-analytical technique known as the differential transform method (DTM) in this research. In 1986, Zhou first introduced DTM [26]. The multi-step differential transformation approach (MS-DTM) is a dependable semi-analytical method that is an excellent enhancement over the traditional DTM. The differential transformation method (DTM) can be applied directly to nonlinear differential equations without requiring linearization and discretization; therefore, it is not affected by errors associated with discretization. Unlike other methods, DTM is independent of any small or large quantities. Therefore, DTM can be applied, where or not governing equations and boundary/initial conditions of a given nonlinear problem contain small or large quantities. Unlike the homotopy analysis method (HAM), DTM does not need to calculate the auxiliary parameter Z_1 ; moreover, through h-curves, DTM does not need initial guesses, an auxiliary linear operator, and solves equations directly. Furthermore, Odibat et al. [27] demonstrated the MS-DTM and its application to chaotic or non-chaotic systems. Further work was carried out by Hasona et al. [28,29], Tripathi et al. [30], Hatami et al. [31], and Beg et al. [32] to solve non-linear ODE and PDE.

In present paper, the impact of the magnetic field, Darcy number, nonlinear convection, thermophoresis, and Brownian motion parameters on double-diffusive MHD transport of a Jeffrey nanofluid through a flexible channel with permeable walls is studied. Non-linear governing equations are solved using MS-DTM. In constrat, Ganesan et al. [14], Raju et al. [15], and Asha et al. [16] analysed the impact of induced Brownian motion, thermophoresis, and magnetic fields on double-stratified nonlinear convective-radiative through analytical results by considering a Jeffrey nanofluid as non-Newtonian fluid. The semi-analytical results of double-diffusive convective flow by considering non-Newtonian fluid through a permeable wall with flexible channel have not yet been studied. The physical parameters of temperature, concentration, velocity, and volume fraction are debated by drawing the graphs. The results obtained by MS-DTM have been compared with the results obtained by NDSolve in Mathematica software and with the finite element method (FEM). The present results have broad biological applications, including biomicrofluidic devices that regulate fluid flow through flexible endoscopes and other medical pumping systems.

2. Mathematical Formulation

Consider a Jeffrey nanofluid peristaltic movement in a two-dimensional flexible channel propagating a sinusoidal wave towards its permeable walls. Using the Cartesian coordinate system (\tilde{X}, \tilde{Y}) , the physical configuration of the channel wall surface is shown in Figure 1 [33].

$$h(\tilde{X}, \tilde{t}) = a(\tilde{X}) + b \sin\left(\frac{2\pi}{\lambda}(\tilde{X} - c\tilde{t})\right) \quad (1)$$

where $a(\tilde{X})$ represents the channel half-width, b indicates wave amplitude, λ denotes the length of the wave, c denotes velocity propagation, and \tilde{t} denotes time.

Let \tilde{U} and \tilde{V} be the velocity parameters, respectively, then the velocity field V can be defined as:

$$V = (\tilde{U}, \tilde{V}, 0) \quad (2)$$

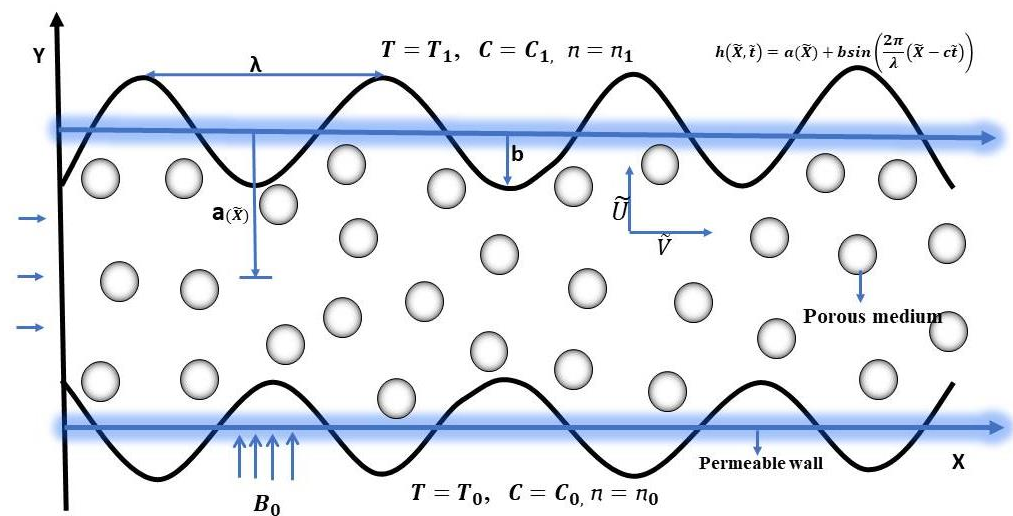


Figure 1. Geometry of the physical model.

For a Jeffrey fluid, the constitutive equations are [4–8]

$$T = -pI + S \tag{3}$$

$$S = \frac{\mu}{1 + \lambda_1} \left(A_1 + \lambda_2 \left(\frac{\partial A_1}{\partial t} + V \cdot \nabla \right) A_1 \right) \tag{4}$$

The Rivlin–Ericksen tensor A_1 is defined through $A_1 = \nabla V + (\nabla V)^T$. Here, I represents the identity tensor, p represents the pressure, λ_1 denotes the ratio between relaxation and retardation times, λ_2 denotes the retardation time, μ is the fluid’s viscosity coefficient, S and T are the extra stress tensor and Cauchy stress tensor, respectively.

The governing equations of a Jeffrey nanofluid are given as [14,15]

$$\frac{\partial \tilde{U}}{\partial \tilde{X}} + \frac{\partial \tilde{U}}{\partial \tilde{Y}} = 0 \tag{5}$$

$$\rho_f \left(\frac{\partial \tilde{U}}{\partial \tilde{t}} + \tilde{U} \frac{\partial \tilde{U}}{\partial \tilde{X}} + \tilde{V} \frac{\partial \tilde{U}}{\partial \tilde{Y}} \right) = -\frac{\partial \tilde{p}}{\partial \tilde{X}} + \frac{\partial \tilde{s}_{xy}}{\partial \tilde{Y}} + \frac{\partial \tilde{s}_{xx}}{\partial \tilde{X}} - \sigma * B_0^2 \tilde{U} - \frac{\mu}{\kappa_0} \tilde{U} + \rho_f g (\tilde{T} - \tilde{T}_0) + \rho_f g (\tilde{C} - \tilde{C}_0) - (\rho_p - \rho_f) g (\tilde{n} - \tilde{n}_0) , \tag{6}$$

$$\rho_f \left(\frac{\partial \tilde{V}}{\partial \tilde{t}} + \tilde{U} \frac{\partial \tilde{V}}{\partial \tilde{X}} + \tilde{V} \frac{\partial \tilde{V}}{\partial \tilde{Y}} \right) = -\frac{\partial \tilde{p}}{\partial \tilde{Y}} + \frac{\partial \tilde{s}_{xx}}{\partial \tilde{X}} + \frac{\partial \tilde{s}_{xy}}{\partial \tilde{Y}} - \sigma * B_0^2 \tilde{V} \tag{7}$$

$$(\rho c)_f \left(\frac{\partial \tilde{T}}{\partial \tilde{t}} + \tilde{U} \frac{\partial \tilde{T}}{\partial \tilde{X}} + \tilde{V} \frac{\partial \tilde{T}}{\partial \tilde{Y}} \right) = k_T \left(\frac{\partial^2 \tilde{T}}{\partial \tilde{X}^2} + \frac{\partial^2 \tilde{T}}{\partial \tilde{Y}^2} \right) + \frac{D_{TC} \alpha c_p}{C_s} \left(\frac{\partial^2 \tilde{C}}{\partial \tilde{X}^2} + \frac{\partial^2 \tilde{C}}{\partial \tilde{Y}^2} \right) - \frac{\partial q_r}{\partial \tilde{Y}} + (\rho c)_p D_B \left(\frac{\partial \tilde{n}}{\partial \tilde{X}} \frac{\partial \tilde{T}}{\partial \tilde{X}} + \frac{\partial \tilde{n}}{\partial \tilde{Y}} \frac{\partial \tilde{T}}{\partial \tilde{Y}} \right) + (\rho c)_p \left(\left(\frac{\partial \tilde{T}}{\partial \tilde{X}} \right)^2 + \left(\frac{\partial \tilde{T}}{\partial \tilde{Y}} \right)^2 \right) \frac{D_T}{T_m} , \tag{8}$$

$$\frac{\partial \tilde{C}}{\partial \tilde{t}} + \tilde{U} \frac{\partial \tilde{C}}{\partial \tilde{X}} + \tilde{V} \frac{\partial \tilde{C}}{\partial \tilde{Y}} = D_{CT} \left(\frac{\partial^2 \tilde{C}}{\partial \tilde{X}^2} + \frac{\partial^2 \tilde{C}}{\partial \tilde{Y}^2} \right) + \left(\frac{\partial^2 \tilde{T}}{\partial \tilde{X}^2} + \frac{\partial^2 \tilde{T}}{\partial \tilde{Y}^2} \right) D_s , \tag{9}$$

$$\frac{\partial \tilde{n}}{\partial \tilde{t}} + \tilde{U} \frac{\partial \tilde{n}}{\partial \tilde{X}} + \tilde{V} \frac{\partial \tilde{n}}{\partial \tilde{Y}} = D_B \left(\frac{\partial^2 \tilde{n}}{\partial \tilde{X}^2} + \frac{\partial^2 \tilde{n}}{\partial \tilde{Y}^2} \right) + \frac{D_T}{T_m} \left(\frac{\partial^2 \tilde{T}}{\partial \tilde{X}^2} + \frac{\partial^2 \tilde{T}}{\partial \tilde{Y}^2} \right) \tag{10}$$

where ρ_p denotes the mass density of nanoparticles, ρ_f denotes the fluid’s effective density, $(\rho c)_f$ and $(\rho c)_p$ are the fluid’s heat capacity and the nanoparticle material’s effective heat capacity, respectively, k_T is the fluid’s thermal conductivity, g is the gravity because of acceleration. Further, D_s denotes the solutal diffusivity, K_0 is the porous medium’s permeability

constant, C_p denotes specific heat at constant pressure, and C_s denotes susceptibility of concentration.

The relationship between the laboratory frame and wave frame is defined by:

$$\tilde{u}(\tilde{x}, \tilde{y}) = \tilde{U} - c, \quad \tilde{v}(\tilde{x}, \tilde{y}) = \tilde{V}, \quad \tilde{x} = \tilde{X} - c\tilde{t}, \quad \tilde{y} = \tilde{Y}, \tag{11}$$

where (\tilde{u}, \tilde{v}) are velocity components, and are coordinated in a wave frame.

Corresponding boundary conditions are given as below:

$$\left. \begin{aligned} |\tilde{u} = -1 - \sqrt{D_a} \frac{\partial^2 \tilde{\psi}}{\partial \tilde{y}^2}, \quad \frac{\partial^2 \tilde{\psi}}{\partial \tilde{y}^2} = 0, \quad \tilde{T} = \tilde{T}_0, \quad \tilde{C} = \tilde{C}_0, \quad \tilde{n} = \tilde{n}_0 \text{ at } \tilde{y} = 0, \\ |\tilde{u} = -1 + \sqrt{D_a} \frac{\partial^2 \tilde{\psi}}{\partial \tilde{y}^2}, \quad \tilde{T} = \tilde{T}_1, \quad \tilde{C} = \tilde{C}_1, \quad \tilde{n} = \tilde{n}_1 \text{ at } \tilde{y} = \tilde{h} = a(\tilde{x}) + b \sin \frac{2\pi}{\lambda}(\tilde{x} - c\tilde{t}) \end{aligned} \right\} \tag{12}$$

Introducing the non-dimensional quantities of the following:

$$\left. \begin{aligned} x = \frac{\tilde{x}}{\lambda}, \quad y = \frac{\tilde{y}}{a}, \quad t = \frac{c\tilde{t}}{\lambda}, \quad M = \sqrt{\frac{\sigma^*}{\mu}} B_0 a, \quad p = \frac{a^2 \tilde{p}}{c\lambda\mu}, \quad v = \frac{\tilde{v}}{c}, \quad u = \frac{\tilde{u}}{c}, \quad h = \frac{\tilde{h}}{a}, \quad \delta = \frac{a}{\lambda}, \quad P_r = \frac{\mu}{\alpha} \\ R_e = \frac{\rho_f c a}{\mu}, \quad \alpha = \frac{k_T}{(\rho c)_f}, \quad \Omega = \frac{\tilde{C} - \tilde{C}_0}{\tilde{C}_1 - \tilde{C}_0}, \quad \theta = \frac{\tilde{T} - \tilde{T}_0}{\tilde{T}_1 - \tilde{T}_0}, \quad \chi = \frac{\tilde{n} - \tilde{n}_0}{\tilde{n}_1 - \tilde{n}_0}, \quad R_d = \frac{16\sigma^* \tilde{T}^3}{3k^* k_t}, \quad D_a = \frac{k_0}{a^2} \\ G_{rT} = \frac{\rho_f g a^2 (\tilde{T}_1 - \tilde{T}_0)}{c\mu}, \quad G_{rC} = \frac{\rho_f g a^2 (\tilde{C}_1 - \tilde{C}_0)}{c\mu}, \quad G_{rF} = \frac{(\rho_p - \rho_f) g a^2 (\tilde{n}_1 - \tilde{n}_0)}{c\mu} \\ N_{TC} = \frac{D_{TC} \alpha c_p (\tilde{C}_1 - \tilde{C}_0)}{\mu k_T c_S (\tilde{T}_1 - \tilde{T}_0)}, \quad N_{CT} = \frac{D_{CT} (\tilde{T}_1 - \tilde{T}_0)}{D_S (\tilde{n}_1 - \tilde{n}_0)}, \quad N_t = \frac{(\rho c)_p D_T (\tilde{T}_1 - \tilde{T}_0)}{(\rho c)_f T_m \mu}, \\ N_b = \frac{(\rho c)_p D_B (\tilde{n}_1 - \tilde{n}_0)}{(\rho c)_f \mu} \quad h = \frac{\tilde{h}}{a} = 1 + \phi \sin 2\pi x, \quad \phi = \frac{b}{a}, \quad f^* = \frac{q}{ca}, \quad u = \frac{\partial \psi}{\partial y}, \quad v = -\delta \frac{\partial \psi}{\partial y}. \end{aligned} \right\} \tag{13}$$

Using the above variables with no dimension, the fundamental Equations (5)–(10) can be reduced to:

$$\frac{\partial p}{\partial x} = \frac{1}{1 + \lambda_1} \frac{\partial^3 \psi}{\partial y^3} - (M^2 + \frac{1}{D_a}) \frac{\partial \psi}{\partial y} + G_{rT} \theta + G_{rC} \Omega - G_{rF} \chi, \tag{14}$$

$$\frac{\partial p}{\partial y} = 0, \tag{15}$$

$$\frac{\partial^2 \theta}{\partial y^2} + N_b P_r \frac{\partial \theta}{\partial y} \frac{\partial \chi}{\partial y} + N_t P_r \left(\frac{\partial \theta}{\partial y} \right)^2 + R_d \frac{\partial^2 \theta}{\partial y^2} + N_{TC} P_r \frac{\partial^2 \Omega}{\partial y^2} = 0, \tag{16}$$

$$\frac{\partial^2 \Omega}{\partial y^2} + N_{CT} \frac{\partial^2 \theta}{\partial y^2} = 0, \tag{17}$$

$$\frac{\partial^2 \chi}{\partial y^2} + \frac{N_t}{N_b} \frac{\partial^2 \theta}{\partial y^2} = 0 \tag{18}$$

Removing pressure from Equations (14) and (15), gives:

$$\frac{1}{1 + \lambda_1} \frac{\partial^4 \psi}{\partial y^4} - (M^2 + \frac{1}{D_a}) \frac{\partial^2 \psi}{\partial y^2} + G_{rT} \theta + G_{rC} \Omega - G_{rF} \chi = 0 \tag{19}$$

The boundary conditions with no dimension in the problem’s wave frame are:

$$\left. \begin{aligned} \psi = 0, \quad u = \frac{\partial \psi}{\partial y} = -1 - \sqrt{D_a} \frac{\partial^2 \psi}{\partial y^2}, \quad \frac{\partial^2 \psi}{\partial y^2} = 0, \quad \theta = 0, \quad \Omega = 0, \quad \chi = 0 \text{ at } y = 0, \\ \psi = f^*, \quad u = \frac{\partial \psi}{\partial y} = -1 + \sqrt{D_a} \frac{\partial^2 \psi}{\partial y^2}, \quad \theta = 1, \quad \Omega = 1, \quad \chi = 1 \text{ at } y = h = 1 + \phi \sin 2\pi x \end{aligned} \right\} \tag{20}$$

Here, the mean flow f^* over a period is considered as:

$$\Theta = f^* + 1, \quad f^* = \int_0^h \frac{\partial \psi}{\partial y} dy \tag{21}$$

where $\Theta = \frac{Q}{ca}$ and $f^* = \frac{Q}{ca}$.

The skin friction coefficient (wall shear stress), Nusselt number (heat transfer rate), and Sherwood number (mass transfer rate) are presented in the following forms [34,35]:

$$C_f = -\frac{\partial u}{\partial y} \Big|_{y=h} \tag{22}$$

$$Nu = -\frac{\partial \theta}{\partial y} \Big|_{y=h} \tag{23}$$

$$Sh = -\frac{\partial \Omega}{\partial y} \Big|_{y=h} \tag{24}$$

Method of Solution

Using MS-DTM with symbolic Mathematica, Equations (16) to (19) are computed with boundary conditions (20). Details for the MS-DTM can be found in the references [26–32].

$$\left(\frac{1}{1+\lambda_1}\right)(k+1)(k+3)(k+2)(k+4)\Psi(k+4) + \Theta(k+1)G_{rT}(k+1) + \Phi(k+1)G_{rC}(k+1) - Y(k+1)G_{rF}(k+1) - (k+1)(k+2)\left(M^2 + \frac{1}{D_a}\right)\Psi(k+2) = 0, \tag{25}$$

$$(k+1)(k+2)\Theta(k+2) + N_b P_r \sum_{r=0}^k \Theta(k+1)(k+1)(k-r+1)Y(k-r+1) + N_{TC} P_r (k+1)(k+2)\Phi(k+2) \tag{26}$$

$$+ R_d(k+1)(k+2)\Theta(k+2) + N_t P_r \sum_{r=0}^k \Theta(k+1)(k+1)(k-r+1)\Theta(k-r+1) = 0, \tag{27}$$

$$(k+1)(k+2)\Phi(k+2) + N_{CT}(k+1)(k+2)\Theta(k+2) = 0, \tag{28}$$

$$(k+1)(k+2)Y(k+2) + \frac{N_t}{N_b}(k+1)(k+2)\Theta(k+2) = 0$$

where $\Psi[k]$, $\Theta[k]$, $\Phi[k]$, and $Y[k]$ are the differential transformation functions of $\psi(y)$, $\theta(y)$, $\Omega(y)$, and $\chi(y)$, respectively, and given as:

$$\psi(y) \cong \sum_{k=0}^m \Psi(k)y^k \tag{29}$$

$$\theta(y) \cong \sum_{k=0}^m \Theta(k)y^k \tag{30}$$

$$\Omega(y) \cong \sum_{k=0}^m \Phi(k)y^k \tag{31}$$

$$\chi(y) \cong \sum_{k=0}^m Y(k)y^k \tag{32}$$

The transformed forms of boundary conditions are as follows:

$$\left. \begin{aligned} \Psi(0) = 0, \quad \Psi(1) = -1, \quad \Psi(2) = 0, \quad \Psi(3) = \frac{m_1}{6}, \quad \Theta(0) = 0, \quad \Theta(1) = m_2, \\ \Phi(0) = 0, \quad \Phi(1) = m_3, \quad Y(0) = 0, \quad Y(1) = m_4. \end{aligned} \right\}$$

where m_1, m_2, m_3, m_4 are unknown coefficients that must be determined.

Substituting Equation (32) into Equations (25)–(28), and other values of $\Psi[k]$, $\Theta[k]$, $\Phi[k]$, and $Y[k]$ can be determined by a recursive method. Hence, substitute all $\Psi[k]$, $\Theta[k]$, $\Phi[k]$, and $Y[k]$ into Equations (29)–(31), We have series solutions given as:

$$\psi(y) = (-1)y + \frac{m_1}{6}y^3 + \frac{1}{1+\lambda_1}(-G_{rT}m_2 - G_{rC}m_3 + G_{rF}m_4)y^4 + \frac{(1+\lambda_1)}{60} \left\{ \frac{(-G_{rT}+G_{rC}N_{CT}-G_{rF}\frac{N_t}{N_b})}{2(1+R_d)}(-N_b P_r m_2 m_4 - 2N_{TC} P_r m_3 - N_t P_r m_2^2) + \frac{m_1}{2}\left(M^2 + \frac{1}{D_a}\right) \right\} y^5 + \dots \tag{33}$$

$$\theta(y) = m_2y + \frac{(-N_bPrm_2m_4 - 2N_{TC}Prm_3 - N_tPrm_2^2)}{2(1+R_d)}y^2 + \frac{Pr(-N_bPrm_2m_4 - 2N_{TC}Prm_3 - N_tPrm_2^2)}{(6(1+R_d)((1+R_d) + N_{TC}N_{CT}Pr))} \left\{ -N_b \left[2 \frac{N_t}{N_b} \left(\frac{(-N_bPrm_2m_4 - 2N_{TC}Prm_3 - N_tPrm_2^2)}{2(1+R_d)} + m_4 \right) \right] - N_t \left(2 \frac{(-N_bPrm_2m_4 - 2N_{TC}Prm_3 - N_tPrm_2^2)}{2(1+R_d)} + m_2 \right) \right\} y^3 + \dots \tag{34}$$

$$\Omega(y) = m_3y + \frac{N_{CT}(-N_bPrm_2m_4 - 2N_{TC}Prm_3 - N_tPrm_2^2)}{2(1+R_d)}y^2 - N_{CT} \frac{Pr(-N_bPrm_2m_4 - 2N_{TC}Prm_3 - N_tPrm_2^2)}{(6(1+R_d)((1+R_d) + N_{TC}N_{CT}Pr))} \left\{ -N_b \left[2 \frac{N_t}{N_b} \left(\frac{(-N_bPrm_2m_4 - 2N_{TC}Prm_3 - N_tPrm_2^2)}{2(1+R_d)} + m_4 \right) \right] - N_t \left(2 \frac{(-N_bPrm_2m_4 - 2N_{TC}Prm_3 - N_tPrm_2^2)}{2(1+R_d)} + m_2 \right) \right\} y^3 + \dots \tag{35}$$

$$\chi(y) = m_4y + \frac{N_t(N_bPrm_2m_4 + 2N_{TC}Prm_3 + N_tPrm_2^2)}{2N_b(1+R_d)}y^2 - \left(\frac{N_t}{N_b} \right) \frac{Pr(-N_bPrm_2m_4 - 2N_{TC}Prm_3 - N_tPrm_2^2)}{(6(1+R_d)((1+R_d) + N_{TC}N_{CT}Pr))} \left\{ -N_b \left[2 \frac{N_t}{N_b} \left(\frac{(-N_bPrm_2m_4 - 2N_{TC}Prm_3 - N_tPrm_2^2)}{2(1+R_d)} + m_4 \right) \right] - N_t \left(2 \frac{(-N_bPrm_2m_4 - 2N_{TC}Prm_3 - N_tPrm_2^2)}{2(1+R_d)} + m_2 \right) \right\} y^3 + \dots \tag{36}$$

Differentiating Equation (33) partially for y we get the velocity equation as:

$$U(y) = (-1) + \frac{m_3}{1+\lambda}y^2 + \frac{4}{1+\lambda}(-G_{rT}m_2 - G_{rC}m_3 + G_{rF}m_4)y^3 + \frac{5(1+\lambda_1)}{60} \left\{ \frac{(-G_{rT} + G_{rC}N_{CT} - G_{rF} \frac{N_t}{N_b})}{2(1+R_d)} (-N_bPrm_2m_4 - 2N_{TC}Prm_3 - N_tPrm_2^2) + \frac{m_1}{2} \left(M^2 + \frac{1}{D_a} \right) \right\} y^4 + \dots \tag{37}$$

Using boundary conditions of Equation (20) and for:

$$G_{rT} = 0.5, G_{rC} = 0.5, G_{rF} = 0.5, N_{CT} = 0.7, N_{TC} = 0.7, N_b = 0.5, N_t = 0.5, D_a = 10, Pr = 7, \lambda_1 = 0.6, M = 0.2.$$

Using boundary conditions of Equation (20), we obtain the values of:

$$\begin{aligned} m_1 &\rightarrow 9.464766924662431, & m_2 &\rightarrow 0.930588663657573, \\ m_3 &\rightarrow -0.3638757341429297, & m_4 &\rightarrow 0.6218840352126972. \end{aligned}$$

3. Results and Discussion

The study shows the application of double-diffusive convective flow and thermal radiation effects in the peristaltic movement of a nanoliquid through a flexible channel. The results obtained by MS-DTM have been compared with the results obtained by NDSolve in Mathematica software and with FEM. The results matched nicely, as shown in Table 1. Results of the skin friction coefficient C_f , Nusselt number Nu , and Sherwood number Sh obtained by MS-DTM is shown in Table 2. Here, we discuss the development of temperature, velocity, nanoparticle volume fraction, and nanoparticle concentration profiles corresponding to the variation of $D_a, R_d, Pr, G_{rT}, G_{rC}, G_{rF}, N_b$ and N_t using a graphical method.

3.1. Velocity Profile

The effects of D_a, Pr, G_{rF}, G_{rC} and G_{rT} on velocity distribution $u(y)$ are presented in Figure 2a–e. Figure 2a shows that velocity in all the regions of the peristaltic pumping diminishes with increasing values of Darcy number D_a . Physically, in fluid flow, D_a provides less resistance. Figure 2b demonstrates the nature of velocity for different values of the Prandtl number Pr . Physically, low Prandtl numbers indicate high heat diffusivity, whereas high Prandtl numbers indicate progressive momentum. The Prandtl number is always positive to control the force and thermal boundary layer thickness. Figure 2c shows that the velocity in all regions of the peristaltic movement decreases with increase values of G_{rF} . Because of an increase in G_{rF} , the fluid viscosity decreases, resulting in a decrease in velocity. From Figure 2d, it is observed that increases in G_{rC} reduce the velocity of the wall; this affects the shrinkage of the thermal boundary layer. Figure 2e shows that with enhancing values of G_{rT} , the velocity profile decreases. The thermal Grashof number

satisfies the proportionate impact of viscous hydrodynamic force and thermal buoyancy force. As a result, as the G_{rT} increases, the viscosity decreases.

Table 1. Comparison of the velocity distribution $u(y)$ obtained by MS-DTM with NDSolve and FEM solution for $G_{rT} = 0.5, G_{rC} = 0.5, G_{rF} = 0.5, N_{CT} = 0.7, N_{TC} = 0.7, N_b = 0.5, N_t = 0.5, D_a = 10, P_r = 7, \lambda_1 = 0.6, M = 0.2$.

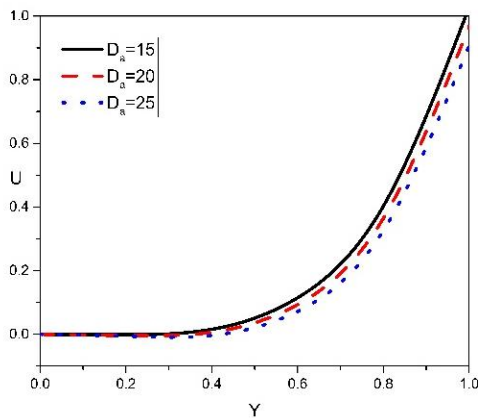
y	Present Result $u(y)$	NDSolve	FEM
0	−1	−1	−1
0.2	−0.987243	−0.98724	−0.987232
0.4	−0.894205	−0.89420	−0.894201
0.6	−0.621413	−0.62141	−0.621411
0.8	−0.0304656	−0.03046	−0.030461
1	1.07577	1	1.004391

Table 2. Results of the skin friction coefficient C_f , Nusselt number N_u , and Sherwood number S_h obtained by MS-DTM. $G_{rT} = 0.5, G_{rC} = 0.5, G_{rF} = 0.5, N_{CT} = 0.7, N_{TC} = 0.7, N_b = 0.5, N_t = 0.5, D_a = 10, P_r = 7, \lambda_1 = 0.6, M = 0.2$.

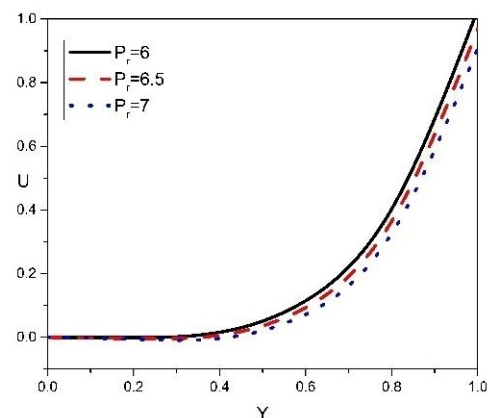
y	Present Result (C_f)	Present Result (N_u)	Present Result (S_h)
0	8.056789	7.098765	−8.0186068
0.2	16.987243	16.189148	−12.073384
0.4	0.8942051	0.384279	−0.00279364
0.6	20.621413	22.585275	−11.602726
0.8	4.0304656	6.792017	−0.00005
1	9.075771	10.00439	−7.0468609

3.2. Temperature Profile

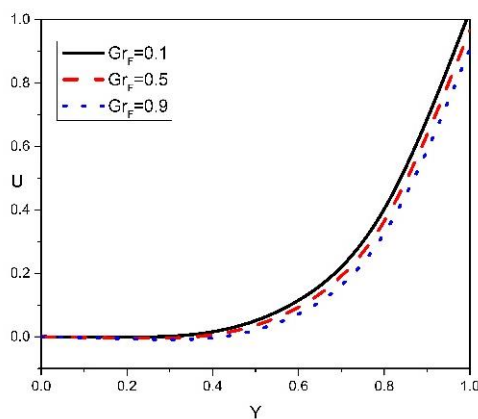
Figure 3a-d were prepared to examine the temperature via R_d, P_r, N_b and N_t . From Figure 3a, it can be seen that temperature in all the regions of peristaltic transport diminishes with enhancing the values of thermal radiation R_d . When the radiation parameter increases, it improves the movement of electromagnetic waves while suppressing heat conduction. Because dispersion heat exchange occurs as a result of irregular atom proliferation, when it is extinguished, the neighbouring particles spread less, and the vitality exchange rate between them becomes less productive. Furthermore, diffusive heat exchange occurs on a longer time scale than radiative heat exchange. Figure 3b demonstrates the nature of temperature distribution for different values of the Prandtl number P_r . Physically, low Prandtl numbers indicate high heat diffusivity, while high Prandtl numbers indicate progressive momentum. The Prandtl number is always positive to control the force and thermal boundary layer thickness. The Brownian motion parameter N_b has an enhancing effect on temperature (see Figure 3c). The Brownian motion of nanofluid particles was proposed because small particles move more uniformly, which may help heat transport. The molecules in the nanofluid grew unpredictably, as did the surrounding fluid particles. Brownian motion describes this. The effects of a Brownian motion-induced molecule were used to increase heat transport between particles and thus the heat radiation of nanofluids. An increase in temperature is observed by enhancing the thermophoresis parameter N_t (see Figure 3d). When the thermophoresis parameter is increased, thermophoretic power is increased due to the mixing of versatile particles, which improves the temperature profile.



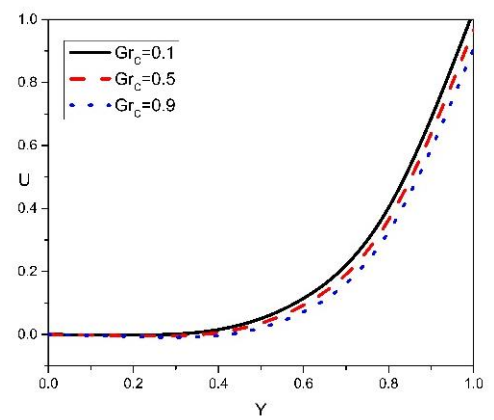
(a)



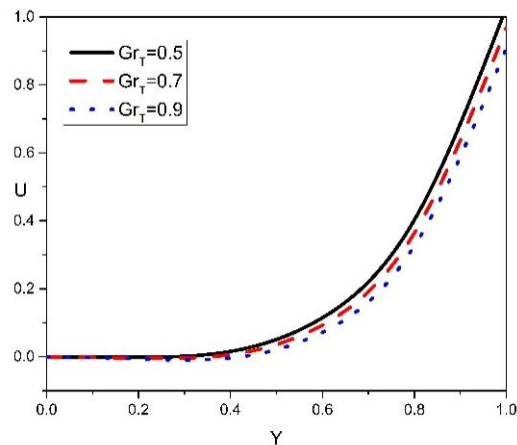
(b)



(c)



(d)



(e)

Figure 2. (a–e) Velocity distribution versus Y for various physical parameters (a) $G_{rT} = 0.5, G_{rC} = 0.5, G_{rF} = 0.5, N_{CT} = 0.7, N_{TC} = 0.7, N_b = 0.5, N_t = 0.5, P_r = 7, \lambda_1 = 0.6, M = 0.2$. (b) $G_{rT} = 0.5, G_{rC} = 0.5, G_{rF} = 0.5, N_{CT} = 0.7, N_{TC} = 0.7, N_b = 0.5, N_t = 0.5, D_a = 10, \lambda_1 = 0.6, M = 0.2$. (c) $G_{rT} = 0.5, G_{rC} = 0.5, N_{CT} = 0.7, N_{TC} = 0.7, N_b = 0.5, N_t = 0.5, D_a = 10, P_r = 7, \lambda_1 = 0.6, M = 0.2$. (d) $G_{rT} = 0.5, G_{rF} = 0.5, N_{CT} = 0.7, N_{TC} = 0.7, N_b = 0.5, N_t = 0.5, D_a = 10, P_r = 7, \lambda_1 = 0.6, M = 0.2$. (e) $G_{rC} = 0.5, G_{rF} = 0.5, N_{CT} = 0.7, N_{TC} = 0.7, N_b = 0.5, N_t = 0.5, D_a = 10, P_r = 7, \lambda_1 = 0.6, M = 0.2$.

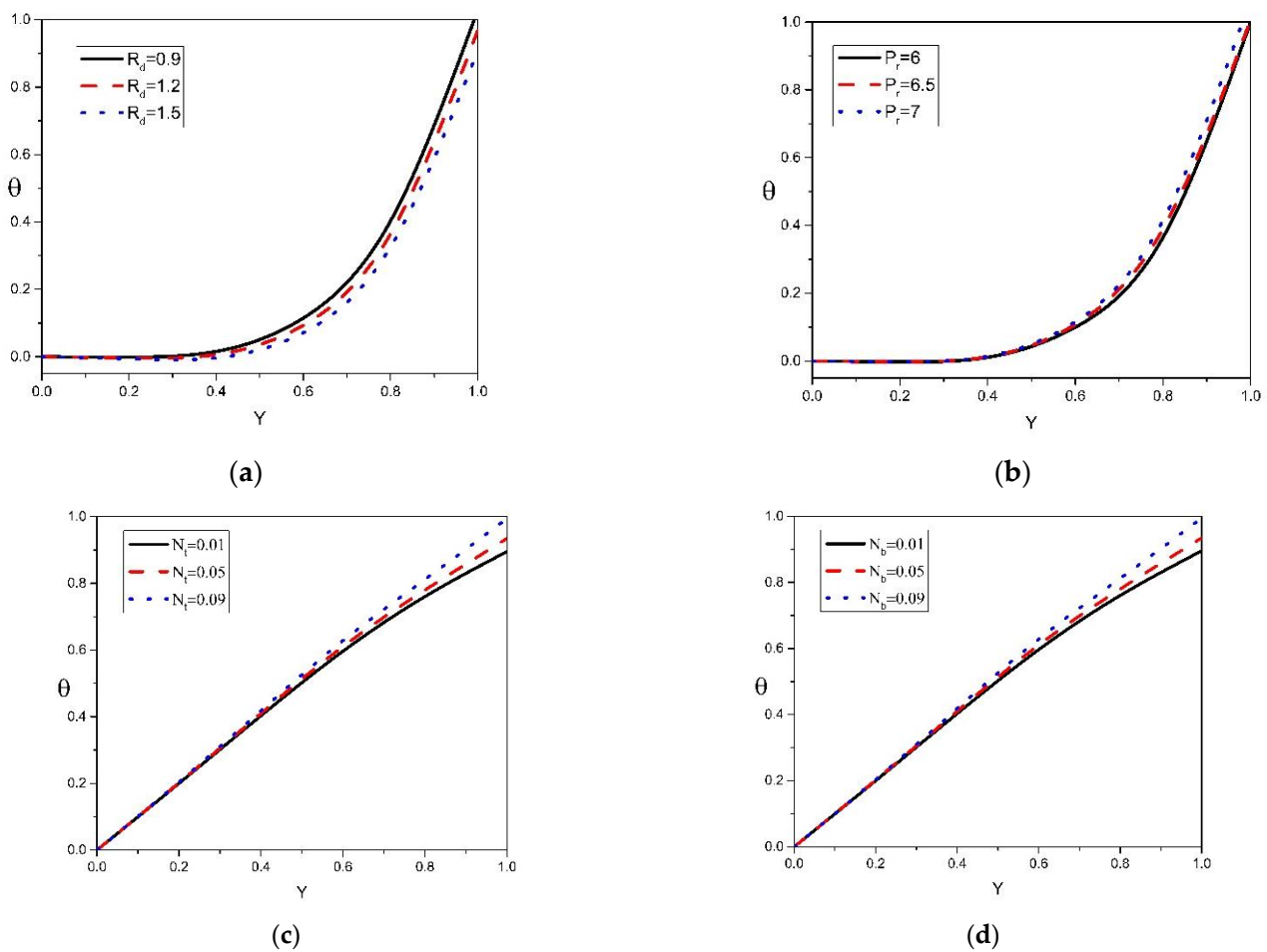


Figure 3. (a–d) Temperature distribution versus Y for various physical parameters (a) $N_{CT} = 0.7, N_{TC} = 0.7, N_b = 0.5, N_t = 0.5, P_r = 7$, (b) $N_{CT} = 0.7, N_{TC} = 0.7, N_b = 0.5, N_t = 0.5, R_d = 0.5$. (c) $N_{CT} = 0.7, N_{TC} = 0.7, R_d = 0.5, N_t = 0.5, P_r = 7$, (d) $N_{CT} = 0.7, N_{TC} = 0.7, N_b = 0.5, R_d = 0.5, P_r = 7$.

3.3. Concentration Profile

Figure 4a–d demonstrate that the concentration profile of the nanoparticles was clarified by the effects of R_d, P_r, N_b and N_t . It is observed from Figure 4a that nanoparticle concentration in all regions of peristaltic movement decreases with increasing values of R_d . R_d is inversely related to the solute concentration, which decreases with the dimensionless transverse coordinate y . Figure 4b demonstrates that as P_r increases, the thermal conductivity of the liquid increases; hence, the concentration of the nanoparticles increases. Figure 4c shows that N_t has a decreasing effect on nanoparticle concentration because of the huge transfer of nanoparticle from a hot region to a cold region, which results a decrease in the concentration distribution. Figure 4d shows that N_b has a decreasing effect on nanoparticle concentration because of the huge transfer of nanoparticle from a hot region to cold region, which results the decrease in concentration distribution.

3.4. Nanoparticle Volume Fraction Profile

Figure 5a–d represent the volume fraction profile of the nanoparticles are presented under the effects of R_d, P_r, N_b and N_t . Figure 5a represents that volume fraction of the nanoparticle in all the regions of the peristaltic pumping diminishes with enhancing the values of R_d . Figure 5b demonstrates the nature of the volume fraction profile of the nanoparticle for various values of P_r . Figure 5c,d show that N_t and N_b have a decreasing effect on nanoparticle volume fraction. Because the temperature distribution in nanofluids

is low, the volume fraction of nanoparticles in the liquid falls as the Brownian motion parameter increases, which might lead to the system's distribution. However, in the case of the thermophoresis parameter, the same findings are observed.

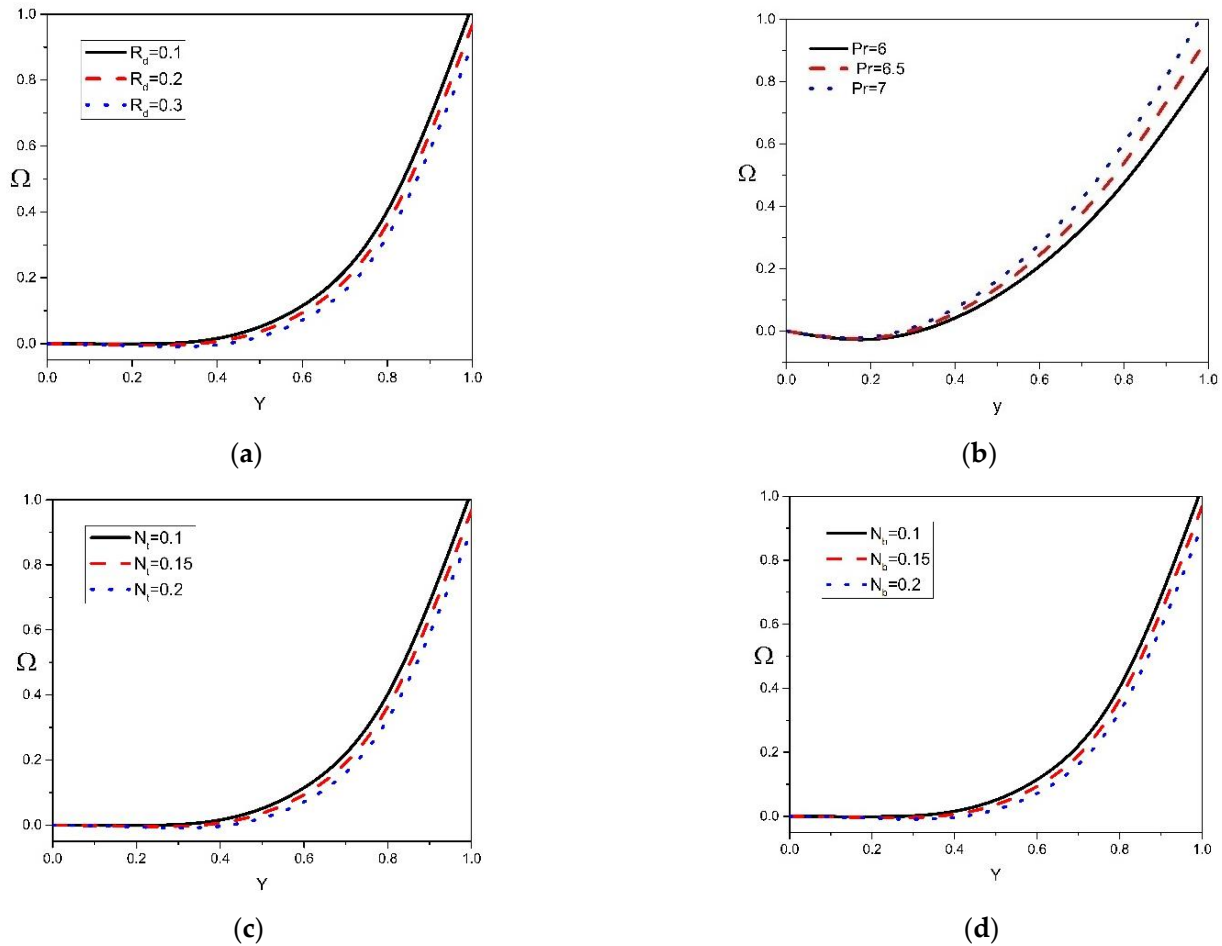


Figure 4. (a–d) Concentration distribution versus Y for various physical parameter (a) $N_{CT} = 0.7, N_{TC} = 0.7, N_b = 0.5, N_t = 0.5, Pr = 7$, (b) $N_{CT} = 0.7, N_{TC} = 0.7, N_b = 0.5, N_t = 0.5, R_d = 0.5$. (c) $N_{CT} = 0.7, N_{TC} = 0.7, R_d = 0.5, N_t = 0.5, Pr = 7$, (d) $N_{CT} = 0.7, N_{TC} = 0.7, N_b = 0.5, R_d = 0.5, Pr = 7$.

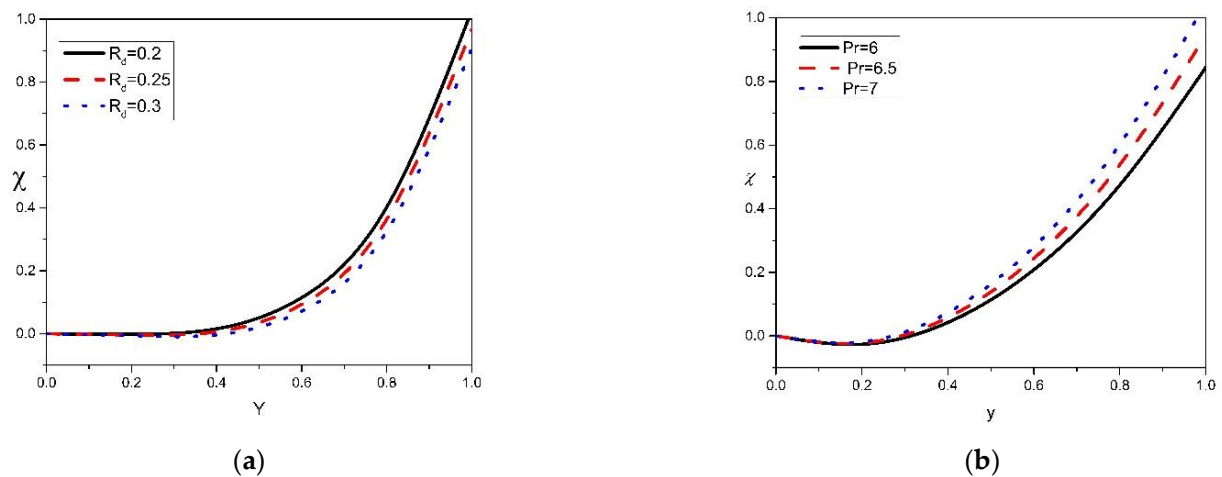


Figure 5. Cont.

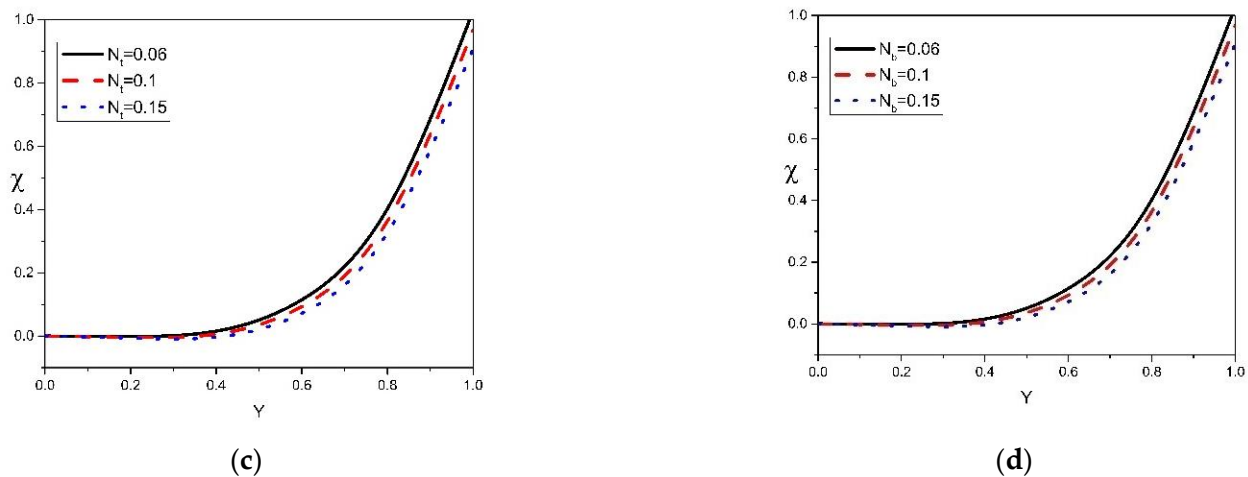


Figure 5. (a–d) Volume fraction distribution versus Y for various physical parameters (a) $N_{CT} = 0.7, N_{TC} = 0.7, N_b = 0.5, N_t = 0.5, P_r = 7$, (b) $N_{CT} = 0.7, N_{TC} = 0.7, N_b = 0.5, N_t = 0.5, R_d = 0.5$. (c) $N_{CT} = 0.7, N_{TC} = 0.7, R_d = 0.5, N_t = 0.5, P_r = 7$, (d) $N_{CT} = 0.7, N_{TC} = 0.7, N_b = 0.5, R_d = 0.5, P_r = 7$.

3.5. Pressure Gradient

Figure 6a–d represent the pressure gradient under the effects of fluid parameter λ_1 , Darcy number D_a , magnetic field M , and solutal Grashof number G_{rC} . Figure 6a shows that the rise in the fluid parameter λ_1 diminishes the pressure gradient. Figure 6b shows that the increase in magnetic field M enhances the pressure gradient. Figure 6c shows that the increase in Darcy number D_a enhances the pressure gradient. Figure 6d indicates that the pressure gradient decreases with the increase in solutal Grashof number G_{rC} i.e., the flow can easily pass without the imposition of a large pressure gradient.

3.6. Trapping Phenomenon

Figures 7–9 represent the Streamline graph under the effects of Jeffery fluid parameter λ_1 , magnetic field M , and Darcy number D_a . An inimitable hydrodynamic property accompanying peristaltic mechanism is the trapping phenomena that occasionally occur when a fluid is subjected to a large amplitude ratio. In the laboratory frame, the set of stream lines represents a fluid bolus moving with and within the wave, and when stream lines bypass the trapped bolus, they attain a shape similar to that of the wall. The development of a flowing bolus by neighbouring stream lines in the direction of fluid flow is termed as trapping. Basically, it is the creation of an internally circulating bolus. The volume of the bolus is defined as the fluid bound by the closed stream lines. This interesting phenomenon is involved in valuable applications in many biological fluids and bioengineering. The flow behaviour of chime in the gastrointestinal tract and the development of thrombus in blood vessels phenomenon followed such interesting applications. Figure 7a–c demonstrate that enhancing the Jeffery fluid parameter λ_1 diminishes the size of the trapped bolus. We observed from Figure 8a–c that the rise in the magnetic field M parameter decreases the size of the trapped bolus. In the figure, it can be seen that the size of the trapped bolus diminishes, and the boluses decrease on cumulative values of the magnetic field parameter M for weak stream line circulation. Thus, the magnetic field force can be used to control bolus formations. In addition, Figure 9a–c show that an increase in Darcy number D_a decreases the magnitude of the bolus.

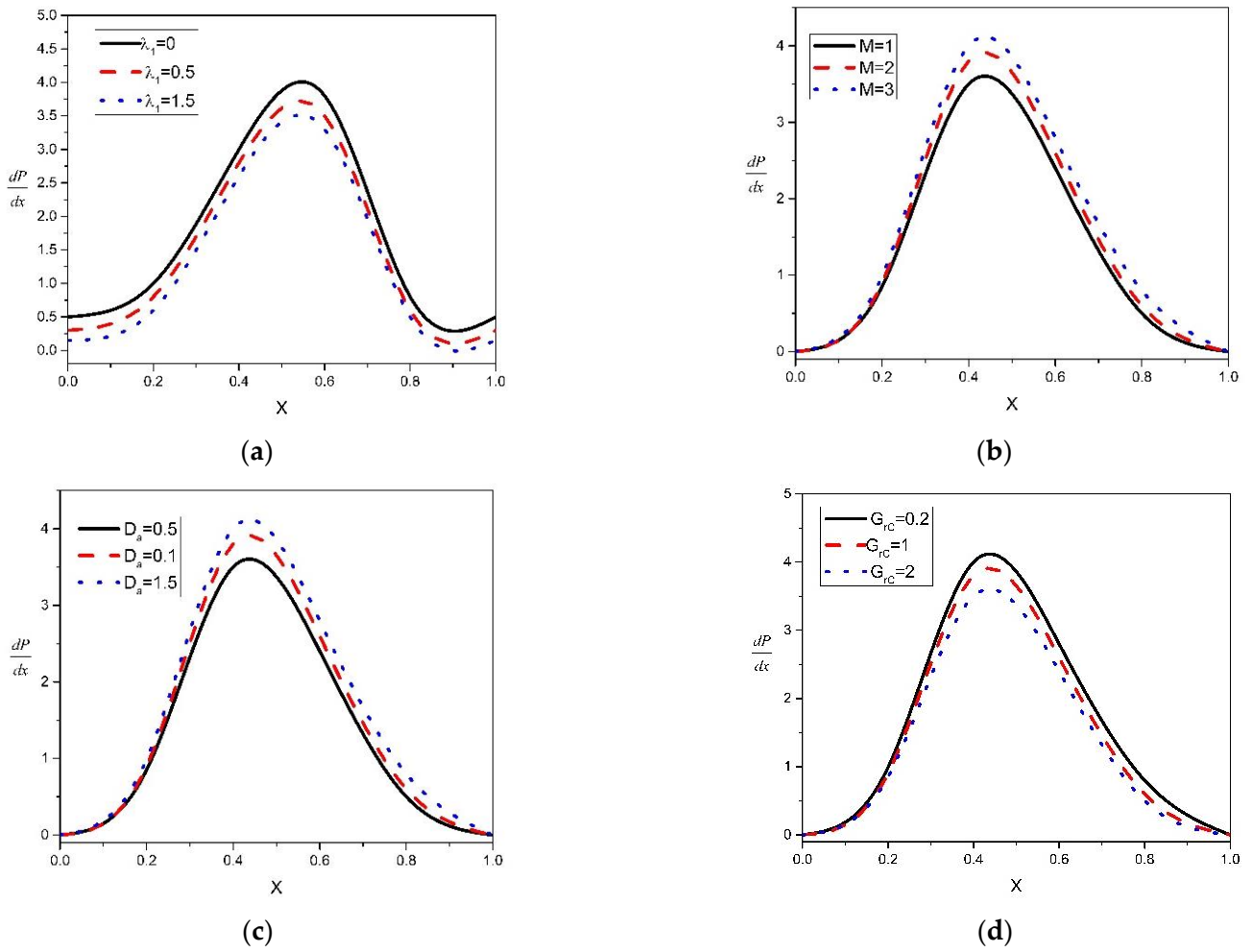


Figure 6. (a–d) Pressure gradient versus X for various physical parameters (a) $G_{rT} = 0.5, G_{rC} = 0.5, G_{rF} = 0.5, Q = -1, D_a = 10, M = 0.2$. (b) $G_{rT} = 0.5, G_{rC} = 0.5, G_{rF} = 0.5, Q = -1, \lambda_1 = 0.6, D_a = 10$. (c) $G_{rT} = 0.5, G_{rC} = 0.5, G_{rF} = 0.5, Q = -1, \lambda_1 = 0.6, M = 0.2$. (d) $G_{rT} = 0.5, G_{rF} = 0.5, D_a = 10, Q = -1, \lambda_1 = 0.6, M = 0.2$.

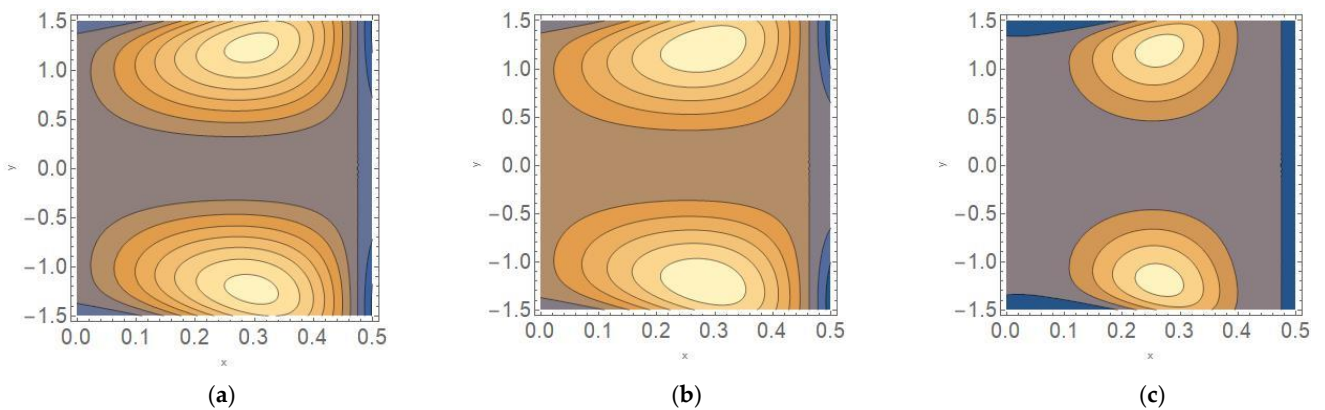


Figure 7. (a–c) Streamlines for (a) $\lambda_1 = 0$, (b) $\lambda_1 = 1$, (c) $\lambda_1 = 2G_{rT} = 0.5, G_{rC} = 0.5, G_{rF} = 0.5, N_{CT} = 0.7, N_{TC} = 0.7, N_b = 0.5, N_t = 0.5, P_r = 7, D_a = 10, M = 0.6$.

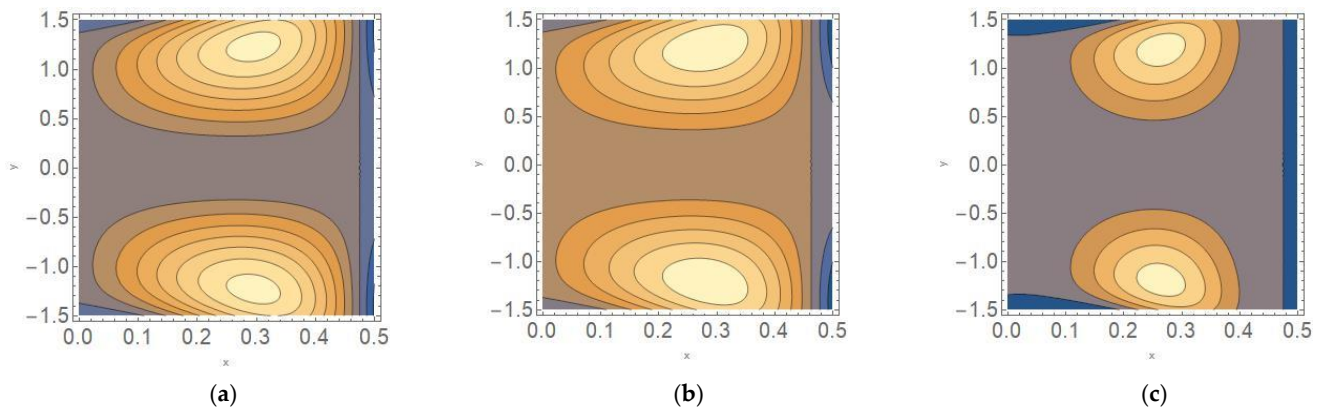


Figure 8. (a–c). Streamlines for (a) $M = 1$, (b) $M = 2$, (c) $M = 3$, $G_{rT} = 0.5$, $G_{rC} = 0.5$, $G_{rF} = 0.5$, $N_{CT} = 0.7$, $N_{TC} = 0.7$, $N_b = 0.5$, $N_t = 0.5$, $P_r = 7$, $D_a = 10$, $\lambda_1 = 0.6$.

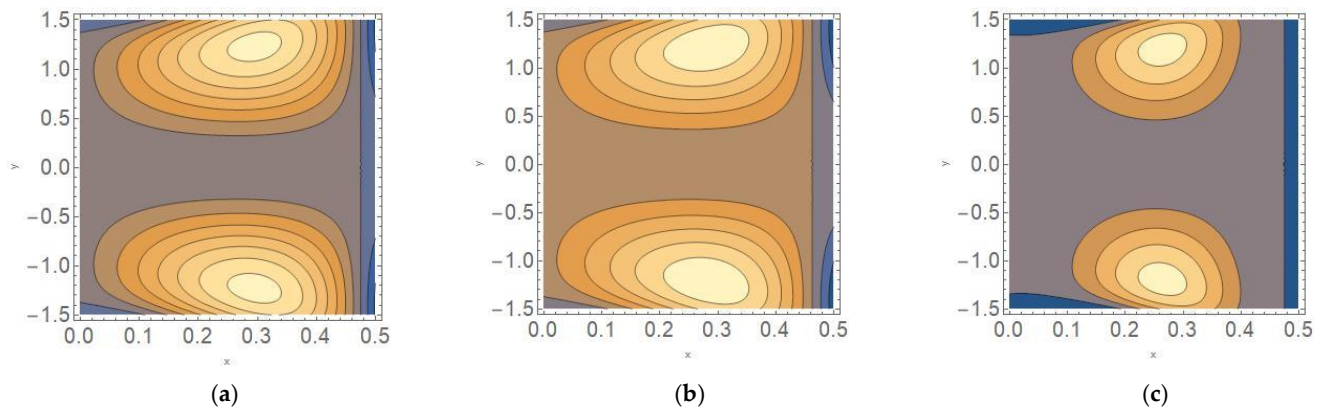


Figure 9. (a–c). Streamlines for (a) $Da = 10$, (b) $Da = 15$, (c) $Da = 20$, $G_{rT} = 0.5$, $G_{rC} = 0.5$, $G_{rF} = 0.5$, $N_{CT} = 0.7$, $N_{TC} = 0.7$, $N_b = 0.5$, $N_t = 0.5$, $P_r = 7$, $M = 0.5$, $\lambda_1 = 0.6$.

4. Conclusions

The current work aims to discuss the double-diffusive convection of a magneto-Jeffrey nanofluid on peristaltic motion under the impact of MHD and a porous medium through a flexible channel with a permeable wall.

The main findings of the paper are as follows.

- 1 The velocity in all the regions of the peristaltic pumping diminishes with increasing values of Darcy number D_a ; in fluid flow, D_a provides less resistance.
- 2 The temperature in all regions of peristaltic transport diminishes with increasing values of thermal radiation R_d .
- 3 Nanoparticle concentration in all regions of the peristaltic movement decreases with enhancing the values of R_d . The R_d is inversely related to the solute concentration, which decreases as the dimensionless transverse coordinate y .
- 4 As P_r increases, the thermal conductivity of the liquid increases; hence, the concentration of nanoparticle increases.
- 5 The volume fraction of the nanoparticle in all regions of peristaltic pumping diminishes with increasing values of R_d .
- 6 In a pressure gradient, the Jeffrey fluid parameter λ_1 , magnetic field M , Darcy number D_a , and solutal Grashof number G_{rC} have the same behaviour.
- 7 Enhancing the Jeffrey fluid parameter λ_1 diminishes the size of the trapped bolus. The increase in the magnetic field M parameter decreases the size of the trapped bolus. In addition, the increase in Darcy number D_a decreases the magnitude of the bolus.

Author Contributions: Conceptualization: A.S.K. and J.B. methodology, A.S.K. and J.B.; formal analyses: I.A.B., S.K., K.H.M.T., N.A.A. Data Curation: J.B., I.A.B., S.K., K.H.M.T., N.A.A., investigation: A.S.K. and J.B.; writing—original draft, A.S.K. and J.B.; resources, I.A.B., S.K., K.H.M.T., N.A.A.; supervision A.S.K., project administration, A.S.K., I.A.B., S.K., N.A.A.; review and editing, I.A.B., S.K., K.H.M.T., N.A.A.; funding, A.S.K., I.A.B., S.K. All authors have read and agreed to the published version of the manuscript.

Funding: This research is funded by King Khalid University.

Institutional Review Board Statement: Not applicable.

Informed Consent Statement: Not applicable.

Data Availability Statement: All data is available in the paper itself.

Acknowledgments: The authors extend their appreciation to the Deanship of Scientific Research at King Khalid University for funding this work through the Large Groups Project under grant number RGP2/101/43. Author Joonabi Beleri would like to thank the Directorate of Minorities for their financial support [DOMWDD/Ph.D//FELLOWSHIP/CR-01/2019-20] Date: 15 October 2019. The authors would like to express their appreciation for the support provided by the Scientific Research Deanship, Islamic University of Madinah.

Conflicts of Interest: We report that we have no potential conflict of interest with any other authors.

Nomenclature

D_T	Thermophoresis diffusion coefficient (m^2s^{-1})
T_m	Fluid mean temperature (K)
τ	Stress tensor (Nm^{-2})
σ	electrical conductivity
D_B	Brownian diffusion coefficient (m^2s^{-1})
\tilde{T}	Temperature of the fluid (K)
$a(\tilde{X})$	Channel half-width (m)
b	Wave amplitude (m)
λ	Wavelength (m)
c	Velocity propagation ($m^{-1}s$)
\tilde{t}	Time (s)
N_{CT}	Soret parameter
e	Electric charge
B_0	Applied magnetic field ($Kgs^{-2}A^{-1}$)
M	Magnetic parameter
I	Identity tensor
p	Pressure
λ_1	The ratio between relaxation and retardation times
λ_2	Retardation time
$\dot{\gamma}$	Shear rate
μ	Fluid viscosity coefficient
S	Extra stress tensor
T	Cauchy stress tensor
ρ_p	Mass density of nanoparticles
ρ_f	Fluid effective density (kgm^{-3})
$(\rho c)_f$	Fluid heat capacity
$(\rho c)_p$	Nanoparticle material's effective heat capacity
k_T	Fluid thermal conductivity ($WK^{-1}m^{-1}$)
g	Acceleration due to gravity (ms^{-1})
D_S	Solutal diffusivity
K_0	Permeability constant ($Wm^{-1}K$)
C_p	Specific heat at constant pressure ($Jkg^{-1}K^{-1}$)
C_s	Susceptibility of concentration
G_{rT}	Thermal Grashof number

R_e	Reynolds number
R_d	Thermal radiation
G_{rT}	Nanoparticle Grashof number
N_b	Brownian motion parameter
P_r	Prandtl number
G_{rC}	Solutal Grashof number
N_{TC}	Dufour parameter
N_t	Thermophoresis diffusion parameter
\tilde{C}	Concentration of fluid
\tilde{n}	Nanoparticle volume fraction
\tilde{X}, \tilde{Y}	Cartesian coordinates

References

- Latham, T.W. Fluid Motion in a Peristaltic Pump. Ph.D. Thesis, Massachusetts Institute of Technology, Cambridge, MA, USA, 1966.
- Shapiro, A.H.; Jaffrin, M.Y.; Weinberg, S.L. Peristaltic pumping with long wavelengths at low Reynolds number. *J. Fluid Mech.* **1969**, *37*, 799–825. [[CrossRef](#)]
- Jaffrin, M.Y.; Shapiro, A.H. Peristaltic pumping. *Annu. Rev. Fluid Mech.* **1971**, *3*, 13–37. [[CrossRef](#)]
- Khan, M.; Iftikhar, F.; Anjum, A. Some unsteady flows of a Jeffrey fluid between two side walls over a plane wall. *Z. Nat. A* **2011**, *66*, 745–752. [[CrossRef](#)]
- Baranovskii, E.S. An inhomogeneous boundary value problem for the stationary motion equations of Jeffreys viscoelastic medium. *J. Appl. Ind. Math.* **2013**, *7*, 22–28. [[CrossRef](#)]
- Baranovskii, E.S. Optimal control for steady flows of the Jeffreys fluids with slip boundary condition. *J. Appl. Ind. Math.* **2014**, *8*, 168–176. [[CrossRef](#)]
- Baranovskii, E.S. Global solutions for a model of polymeric flows with wall slip. *Math. Methods Appl. Sci.* **2017**, *40*, 5035–5043. [[CrossRef](#)]
- Hayat, T.; Ahmad, N.; Ali, N. Effects of an endoscope and magnetic field on the peristalsis involving Jeffrey fluid. *Commun. Nonlinear Sci. Numer. Simul.* **2008**, *13*, 1581–1591. [[CrossRef](#)]
- Choi, S.U.; Eastman, J.A. *Enhancing Thermal Conductivity of Fluids with Nanoparticles*; Argonne National Lab.: Argonne, IL, USA, 1995.
- Akbar, N.S. Peristaltic flow of a nanofluid with slip effect. *Meccanica* **2012**, *47*, 1283–1294. [[CrossRef](#)]
- Ayub, S. Thermal radiation impact in the mixed convective peristaltic flow of third-grade nanofluid. *Results Phys.* **2017**, *7*, 3687–3695. [[CrossRef](#)]
- Asha, S.K.; Beleri, J. Peristaltic flow of Carreau nanofluid in presence of Joule heat effect in an inclined asymmetric channel by multi-step differential transformation method. *World Sci. News* **2022**, *164*, 44–63.
- Aifanties, E.C. Continuum basis for diffusion in regions with multiple diffusivities. *J. Appl. Phys.* **1976**, *50*, 1334–1338. [[CrossRef](#)]
- Ganesan, S.; Vasanthakumari, R. Influence of magnetic field and thermal radiation on peristaltic motion with double-diffusive convection in Jeffery nanofluids. *Heat Transf.* **2020**, *49*, 2025–2043. [[CrossRef](#)]
- Raju, A.; Ojjela, O.; Kambhatla, P.K. The combined effects of induced magnetic field, thermophoresis and Brownian motion on double stratified nonlinear convective-radiative Jeffrey nanofluid flow with heat source/sink. *J. Anal.* **2020**, *28*, 503–532. [[CrossRef](#)]
- Shivappa Kotnurkar, A.; Giddaiah, S. Double diffusion on peristaltic flow of nanofluid under the influences of magnetic field, porous medium, and thermal radiation. *Eng. Rep.* **2020**, *2*, e12111. [[CrossRef](#)]
- Ali, A.; Ali, Y.; Khan Marwat, D.N.; Awais, M.; Shah, Z. Peristaltic flow of nanofluid in a deformable channel with double diffusion. *SN Appl. Sci.* **2020**, *2*, 100. [[CrossRef](#)]
- Sucharitha, G.; Vajravelu, K.; Lakshminarayana, P. Effect of heat and mass transfer on the peristaltic flow of a Jeffrey nanofluid in a tapered flexible channel in the presence of aligned magnetic field. *Eur. Phys. J. Spec. Top.* **2019**, *228*, 2713–2728. [[CrossRef](#)]
- Asha, S.K.; Sunita, G. Influence of thermal radiation on peristaltic blood flow of a Jeffrey fluid with double diffusion in the presence of gold nanoparticles. *Inform. Med. Unlocked* **2019**, *17*, 100272.
- Hussain, Q. Nonlinear radiative peristaltic flow of hydromagnetic fluid through a porous medium. *Results Phys.* **2018**, *9*, 121–134. [[CrossRef](#)]
- Ramesh, K.; Devakar, M. Peristaltic transport of MHD Walters B fluid through porous medium with heat transfer. *Iran. J. Sci. Technol. Trans. A Sci.* **2017**, *41*, 489–504. [[CrossRef](#)]
- Vajravelu, K.; Sreenadh, S.; Lakshminarayana, P.; Sucharitha, G.; Rashidi, M.M. Peristaltic flow of phan- thein-Tanner fluid in an Asymmetric Channel with porous medium. *J. Appl. Fluid Mech.* **2015**, *9*, 1615–1625.
- Maiti, S.; Misra, J.C. Peristaltic flow of a fluid in a porous channel: A study having relevance to flow of bile within ducts in a pathological state. *Int. J. Eng. Sci.* **2011**, *49*, 950–966. [[CrossRef](#)]
- Noreen, S.; Qurat, U. Entropy generation analysis on electroosmotic flow in non-Darcy porous medium via peristaltic pumping. *J. Therm. Anal. Calorim.* **2019**, *137*, 1991–2006. [[CrossRef](#)]

25. Hasona, W.M.; El-Shehkipy, A.A.; Ibrahim, M.G. Combined effects of magnetohydrodynamic and temperature dependent viscosity on peristaltic flow of Jeffrey nanofluid through a porous medium: Applications to oil refinement. *Int. J. Heat Mass Transf.* **2018**, *126*, 700–714. [[CrossRef](#)]
26. Zhou, J.K. *Differential Transformation and Its Applications for Electrical Circuits*; Huazhong University Press: Wuhan, China, 1986; pp. 1279–1289.
27. Odibat, Z.M.; Bertelle, C.; Aziz-Alaoui, M.A.; Duchamp, G.H. A multi-step differential transform method and application to non-chaotic or chaotic systems. *Comput. Math. Appl.* **2010**, *59*, 1462–1472. [[CrossRef](#)]
28. Hasona, W.M.; El-Shehkipy, A.; Ibrahim, M.G. Semi-analytical solution to MHD peristaltic flow of a Jeffrey fluid in presence of Joule heat effect by using multi-step differential transform method. *New Trends Math. Sci.* **2019**, *7*, 123–137. [[CrossRef](#)]
29. Hasona, W.M. Temperature-dependent electrical conductivity and thermal radiation effects on MHD peristaltic motion of Williamson nanofluids in a tapered asymmetric channel. *J. Mech.* **2020**, *36*, 103–118. [[CrossRef](#)]
30. Tripathi, D.; Bég, O.A.; Gupta, P.K.; Radhakrishnamacharya, G.; Mazumdar, J. DTM simulation of peristaltic viscoelastic biofluid flow in asymmetric porous media: A digestive transport model. *J. Bionic Eng.* **2015**, *12*, 643–655. [[CrossRef](#)]
31. Hatami, M.; Ghasemi, S.E.; Sahebi, S.A.R.; Mosayebidorcheh, S.; Ganji, D.D.; Hatami, J. Investigation of third-grade non-Newtonian blood flow in arteries under periodic body acceleration using multi-step differential transformation method. *Appl. Math. Mech.* **2015**, *36*, 1449–1458. [[CrossRef](#)]
32. Bég, O.A.; Keimanesh, M.; Rashidi, M.M.; Davoodi, M.; Branch, S.T. Multi-step DTM simulation of magneto-peristaltic flow of a conducting Williamson viscoelastic fluid. *Int. J. Appl. Math. Mech.* **2013**, *9*, 1–19.
33. Kotnurkar, A.S.; Beleri, J.; Badruddin, I.A.; Kamangar, S.; Ahammad, N.A. Peristaltic Transport of Carreau Nanofluid in Presence of Triple Diffusion in an Asymmetric Channel by Multi-Step Differential Transformation Method. *Mathematics* **2022**, *10*, 807. [[CrossRef](#)]
34. Reddy, K.V.; Reddy, M.G.; Makinde, O.D. Heat and Mass Transfer of a Peristaltic Electro-osmotic Flow of a Couple Stress Fluid through an Inclined Asymmetric Channel with Effects of Thermal Radiation and Chemical Reaction. *Period. Polytech. Mech. Eng.* **2021**, *65*, 151–162. [[CrossRef](#)]
35. Vaidya, H.; Rajashekhar, C.; Prasad, K.V.; Khan, S.U.; Riaz, A.; Viharika, J.U. MHD peristaltic flow of nanofluid in a vertical channel with multiple slip features: An application to chyme movement. *Biomech. Model. Mechanobiol.* **2021**, *20*, 1047–1067. [[CrossRef](#)] [[PubMed](#)]